

Cryo-EM Reveals Architectural Diversity in Active Rotavirus Particles

Mary Hauser^a, William J. Dearnaley^{b,c,d}, A. Cameron Varano^{b,c,d}, Michael Casasanta^{b,c,d}, Sarah M. McDonald^e, Deborah F. Kelly^{b,c,d,*}

^a GeoVax, Inc., Smyrna, GA, USA

^b Department of Biomedical Engineering, Pennsylvania State University, University Park, PA 16802, USA

^c Huck Institutes of the Life Sciences, Pennsylvania State University, University Park, PA 16802, USA

^d Center for Structural Oncology, Pennsylvania State University, University Park, PA 16802, USA

^e Department of Biology, Wake Forest University, Winston-Salem, NC 27109, USA

ARTICLE INFO

Article history:

Received 24 May 2019

Received in revised form 26 July 2019

Accepted 27 July 2019

Available online 31 July 2019

Keywords:

Cryo-Electron microscopy

Rotavirus

Double-layered particle

Activation

ABSTRACT

Rotavirus is a well-studied RNA virus that causes severe gastroenteritis in children. During viral entry, the outer layer of the virion is shed, creating a double-layered particle (DLP) that is competent to perform viral transcription (i.e., mRNA synthesis) and launch infection. While inactive forms of rotavirus DLPs have been structurally characterized in detail, information about the transcriptionally-active DLP remains limited. Here, we used cryo-Electron Microscopy (cryo-EM) and 3D image reconstructions to compare the structures of internal protein components in transcriptionally-active versus inactive DLPs. Our findings showed that transcriptionally-active DLPs gained internal order as mRNA synthesis unfolded, while inactive DLPs remained dynamically disordered. Regions of viral protein/RNA constituents were analyzed across two different axes of symmetry to provide a more comprehensive view of moving components. Taken together, our results bring forth a new view of active DLPs, which may enable future pharmacological strategies aimed at obliterating rotavirus transcription as a therapeutic approach.

© 2019 The Authors. Published by Elsevier B.V. on behalf of Research Network of Computational and Structural Biotechnology. This is an open access article under the CC BY-NC-ND license (<http://creativecommons.org/licenses/by-nc-nd/4.0/>).

1. Introduction

1.1. The Inner-workings of RNA Viruses

RNA viruses cause widespread disease in humans creating significant challenges for medicine and society. Rotaviruses are segmented, double-stranded (ds) RNA viruses of the *Reoviridae* family that are recognized as a leading cause of life-threatening gastroenteritis in young children worldwide [1]. Replication of rotaviruses is tightly controlled through ordered stages of viral particle disassembly and assembly [2]. Despite the disease burden of rotavirus, the molecular mechanisms of RNA synthesis are not fully understood. Mature rotaviruses have a complex icosahedral structure that consists of three concentric protein layers surrounding 11 segments of dsRNA genome. The outermost layer of the virus is shed upon entry into the cell, resulting in a double-layered particle (DLP). The outer layer of the DLP, which retains $T = 13$ icosahedral symmetry, is composed of 260 trimers of VP6 that act to bridge the subunits of the innermost core shell [3]. The $T = 1$

symmetrically mismatched core shell is composed of 120 copies of VP2. The extreme N-terminal residues of VP2 (~1–100) make-up a flexible region that is thought to project into the particle interior along the 5-fold vertices and engage the viral polymerase, VP1, and capping enzyme, VP3 [4]. Following cell entry and shedding of the outer capsid, simultaneous transcription of 11 single-stranded, positive-sense RNAs (i.e., mRNAs) occurs within the intact DLP. In this context, the polymerases use the minus-strands of the dsRNA genome segments as templates [5,6]. After mRNA synthesis, capping is performed by VP3, and the nascent transcripts are extruded through channels at the 5-fold vertices [7].

Although structural information exists for rotavirus DLPs, details of internal protein arrangement have not been fully elucidated [8–10]. Utilizing x-ray crystallography of the inactive DLP, McClain and colleagues described a hub protruding inward at each of the 5-fold axes as a cylindrical feature with rod-like substructures that was attributed to the N-terminal segments of ten VP2 subunits [4]. Further studies revealed that extra density of the 5-fold hub was consistent with a single copy of the viral polymerase, VP1 [11]. When the outermost layer of mature rotavirus dissociates, outward displacement of VP1 occurs and helps contributes to the activation of the polymerase [10,12]. The activity of VP1 is tightly controlled

* Corresponding author at: Department of Biomedical Engineering, Pennsylvania State University, University Park, PA 16802, USA
E-mail address: Debkelly@psu.edu (D.F. Kelly).

by interaction with VP2 [13]. While much is known of the biochemical framework that governs DLP activity [14], the overall internal architectures of these rotavirus disassembly intermediates remain unclear. Such structural information will help clarify molecular insights and may also inform the development of better therapeutic measures to treat rotavirus infection among vulnerable populations.

1.2. Shedding Light on Rotavirus Diversity

In this study, we shed light on the architectural diversity of internal DLP components of simian rotavirus strain SA11 during biochemical activation. Cryo-Electron Microscopy (cryo-EM) of frozen-hydrated active DLPs provided a detailed analysis of changes in viral protein arrangements in comparison to inactive DLPs. We also found that the high density along the 5-fold axis becomes reinforced during transcription, as it builds electron scattering properties. Density changes were prominent surrounding the core and putative VP1/3 subunits when comparing active versus inactive rotavirus DLPs. Taken together, the results highlight the inner-workings of an important viral pathogen during its biochemically relevant infection processes.

2. Results/Discussion

2.1. A Glimpse Inside the DLP Framework

Structural analysis shows that the outer VP6 layer of the DLP undergoes physical changes during transcription; however the organization of viral proteins and RNA within active DLPs is just coming to light [7,10]. We utilized cryo-EM to examine interior virion architecture of both biochemically-active and inactive rotavirus DLPs. Viral

transcription of the dsRNA genome within intact DLPs readily occurs *in vitro* upon the addition of NTPs and Mg^{2+} [15]. Newly synthesized mRNA strands were not observed in samples of inactive DLPs in which NTPs were absent, while strands of mRNA emerging from viral particles are seen in samples containing active DLPs (Fig. 1A, B; white arrows).

3D structures for the transcriptionally-active and inactive DLPs were calculated using the RELION software package [16] and visualized using the UCSF Chimera software program [17]. The inactive DLP structure was derived from 452 particles (equivalent to 27,120 icosahedral particles) and was resolved at ~ 10 -Å. By comparison, the actively-transcribing DLP structure was derived from 467 particles (equivalent to 28,020 icosahedral particles) and was resolved to 12-Å. A computational slice through the density maps revealed the interior composition of the viral particles. To more easily distinguish the protein layers, radial depth-cued coloring was applied and defined by distance in angstroms from the center of the particle based on established techniques [18].

Structural organization begins to differ between active and inactive DLPs beneath VP2, at a radial distance of ~ 260 Å and where VP1/3 and the VP2 N-termini would be located. These differences in structural features persisted inward to the viral interior (Fig. 1; Movies S1, S2). Specifically, the VP1/3 region and VP2 zone show discrete differences in structural orientation between the two density maps, which correlated with differences in their biochemical activity (i.e., active vs. inactive). Among the most notable rearrangements is the defined density at the center of the transcriptionally active DLP compared to the density map of the inactive DLP. This observation suggests that the innermost viral material becomes more structurally ordered during transcription.

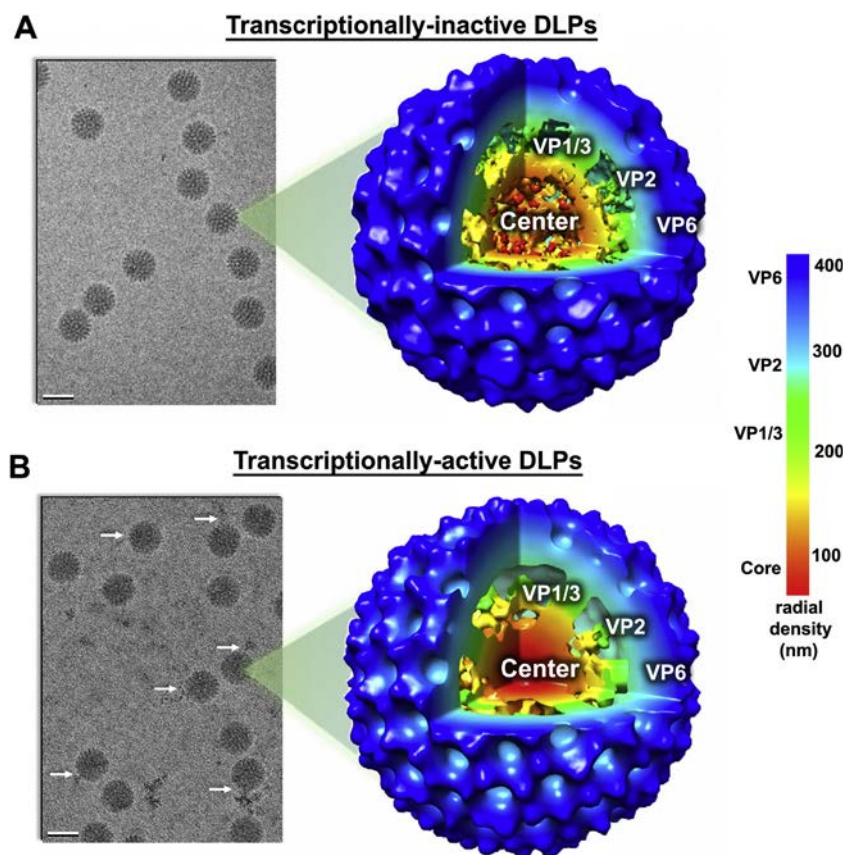


Fig. 1. Rotavirus DLP reconstructions show interior details. EM images of transcriptionally-inactive (A) and transcriptionally-active (B) rotavirus DLPs. White arrows point to newly synthesized mRNAs emerging from the particles. Scale bar is 80 nm. Cryo-EM density maps of rotavirus DLPs with an octant removed aid in the visualization of the particle's interior features. Density maps are colored based on radial depth from the center of the structures. Putative protein components are labeled; VP6 is displayed in dark blue, VP2 in light blue, the VP1/VP3 complex in green, and the core in red.

2.2. At the Cross-section of Active and Inactive States

To better navigate the depths of the DLPs internal features, cross-sections of the 3D structures were analyzed at 50-nm increments. While the exteriors of the density maps show strong similarities, differences in architecture begin to emerge upon traversing the interior components (Fig. 2; Movies S3, S4). A colorized comparison of the central section in the two states was extracted to delineate relative protein density. The 3D reconstructions of both active and inactive DLPs showed high density hubs along the 5-fold axes. This feature is consistent with previous work and has identified the internal projections as VP2 N-termini associated with a complex of VP1/3, the viral polymerase and capping enzyme [4]. In the space surrounding these projections, transcriptionally-active DLPs displayed local high-density features, whereas inactive DLPs exhibited lower density features spanning through the particle interior.

As we approach the center of the DLP, condensed material was present in the active DLPs, which is in contrast to inactive particles within which little to no density was observed at the center of the map. Overall, actively-transcribing DLPs displayed distinct continuity in higher density features along the 5-fold axis as seen at spherical slices and confirmed by radial measurements in the range of 200–120 Å. Again, striking differences were noted within the 90-Å center range. This observation suggests the rearrangement of biological material at the heart of active DLPs presenting a rigid, discernable structure.

To better understand the nuanced structural changes caused by biochemical activation, spherical slices through the reconstructions were analyzed. Specifically, a spherical slicing factor of 0.9 was applied at sequential radial depths from the particle center [19] using the Chimera software package [17]. The slicing procedure forces the removal of the particle capsid while leaving behind a smoothly-rendered surface.

Density for the VP2 layer (red / yellow) is highlighted and present in the transcriptionally-active and inactive DLPs at a radial depth of ~25 nm (Fig. 2B). Interestingly, at this depth, known type II aqueous channels surrounding the 5-fold axes appear more prominent (green) in active DLPs as compared to inactive particles. This observation is consistent with other reports that claim mRNA is extruded from these pores [20]. Reconstructions of both active and inactive particles also display high density along the 5-fold axis. This degree level of order was only deeply consistent in active DLPs up to ~10 nm (Fig. 2A, B). The prominent difference in the core density was noted at and beyond 10 nm in that active DLPs contained a dense particle center, whereas, inactive DLPs displayed a lack of strong density in the same region. These architectural findings show how structural rearrangements are needed for the transcriptional process to unfold.

2.3. Axis of Comparison – 5-fold Versus 2-fold Activities

A broader comparison on the structural rearrangements surrounding the 5-fold and 2-fold symmetry axes helped delineate protein domains. To facilitate this comparison, we performed a cuboid extraction procedure across each of the central sections of the density maps along the axes of interest (Figs. 3, 4). The cuboid, highlighted in red, traversed the VP6 outer shell, through the central core, and extended through the density map, encompassing the VP6 layer on the opposite side of the particle (Fig. 3A; Movie S5, S6). The VP6 layer on both sides of the particle map were clearly defined in the inactive and transcriptionally-active states. Radial measurements defined the segmented region for VP2 adjacent to the VP6 layer, which was also well defined in the active and inactive density maps. A plug at the center domain was well-defined in the active structure, flanked by pentameric-shaped protein motifs, likely comprised of VP1/3 (Fig. 3B).

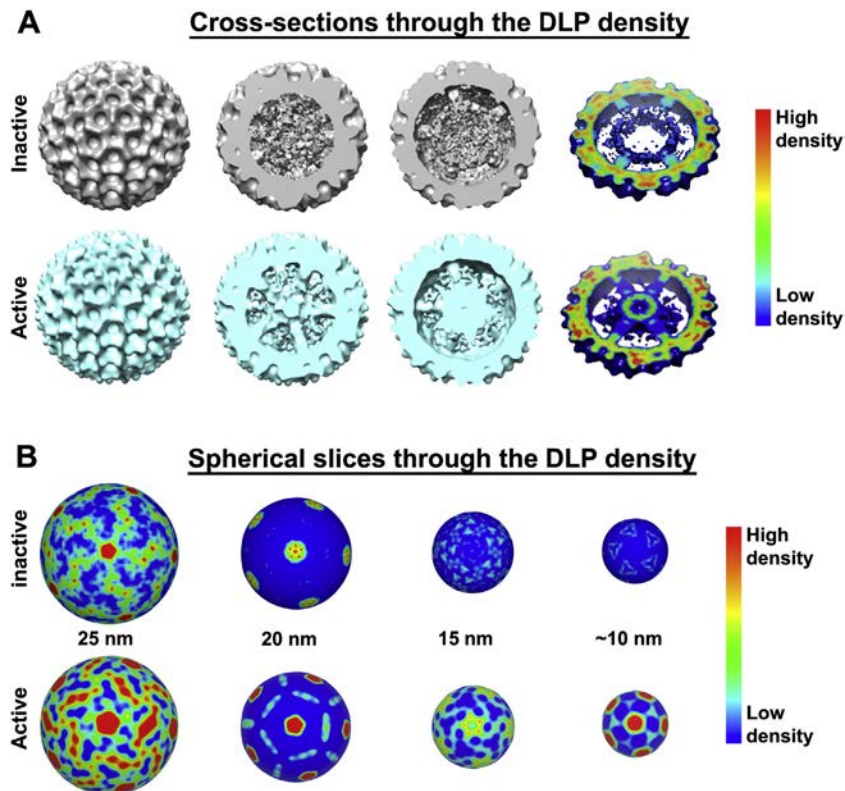


Fig. 2. Cross-sectional views of DLPs indicate variable features in density distribution. (A) EM density maps inactive (gray) and active (blue) rotavirus DLPs are shown were cross-sectioned at 50 nm-increments. Corresponding cross-sections reveal a more ordered central core in active particles compared with inactive structures. Volume density is colored with highest measures of electron density in red and lowest values in blue. (B) Spherical slices show differences between high density features in DLPs reconstructions. The cumulative density is displayed across radial measurements from the center of each density map. Higher density was observed at each layer in the active DLPs structure versus the inactive structure.

Density along the 5-fold axis

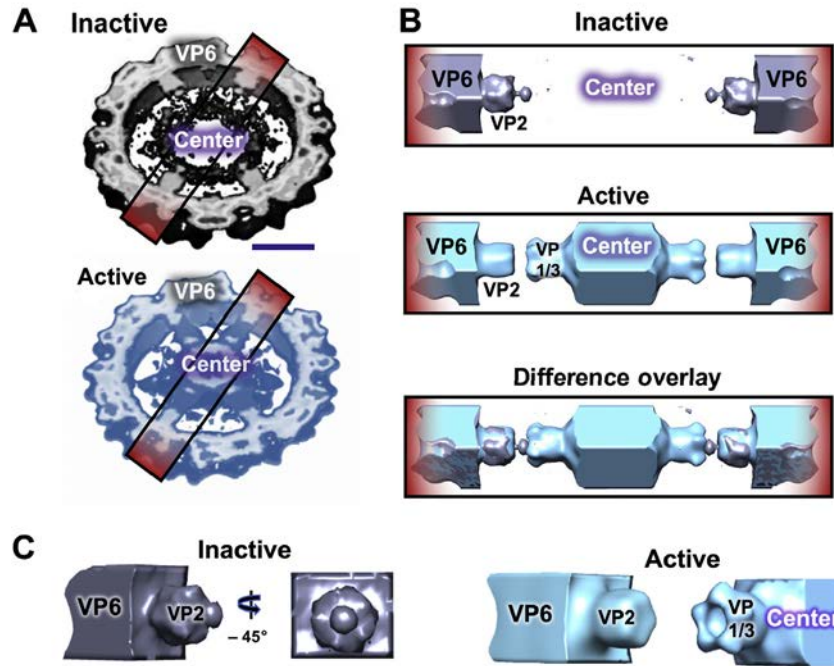


Fig. 3. Interior features of rotavirus DLPs along the 5-fold axes. (A) Central cross-sections of inactive (gray) and transcriptionally-active (blue) DLPs were used as a template for the cuboid extraction procedure (red highlighted section). Scale bar is 20 nm. (B) The resulting cuboid density from the inactive DLP structure displays density present in the region that encompasses VP6 and VP2 according to radial measurements originating from the center of the particle. The cuboidal density was extracted from active DLPs using the same computational procedures. A difference overlay conveys areas of density overlap in the active and inactive structures. (C) Rotational views of the cuboid show structural features in the active particle representative of the VP6, VP2, VP1/3 region and the center domain.

Density along the 2-fold axis

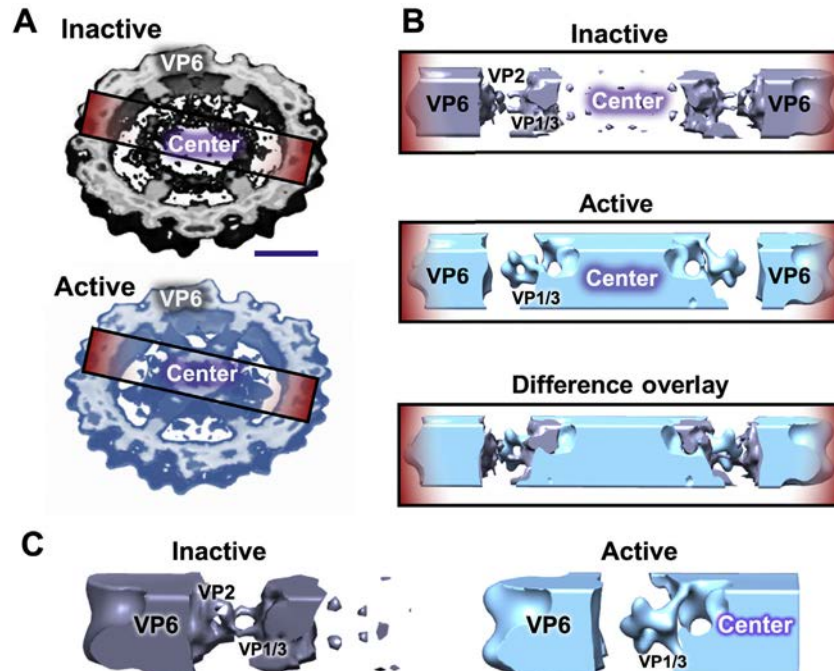


Fig. 4. Interior features of rotavirus DLPs along the 2-fold axis. (A) Central cross-sections of inactive (gray) and transcriptionally-active (blue) DLPs were used as a template for the cuboid extraction procedure (red highlighted section). Scale bar is 20 nm. (B) The cuboid density from the inactive DLP structure shows density that encompasses VP6, VP2, and VP1/3 according to radial measurement originating from the center of the particle. The central core domain is disordered in the inactive structure. The cuboidal density of active DLPs shows density for VP6 and VP1/3 but lacks information for VP2. A difference overlay conveys areas of density that overlaps in the active and inactive structures. (C) Rotational views of the cuboid show structural features in the active particle and the center domain, which is absent from the inactive structure.

Prior work demonstrated that a lack of symmetry constraints during refinement procedures resulted in disordered structures of transcribing DLPs [14]. We achieved higher resolution structures by enforcing icosahedral symmetry. In doing so, the density for the VP1/3 plug was reinforced during consecutive rounds of refinement and visible in multiple classes. Classes lacking enforced symmetry were similar to our previously published disordered structures [14]. A difference map overlay of the inactive and transcriptionally-active cuboid extracts was also performed. Results from this analysis show a strong comparison in the structural density within VP6-VP2 interaction regions (Fig. 3C). Meanwhile, the VP1/3 and center density domains were uniquely ordered in the active structure in comparison with the inactive state. This finding is consistent with the radial analysis and confirms that the active structure adopts a more ordered state as it is biochemically triggered.

Using the same cuboidal extraction procedures, we further examined the density that traversed the 2-fold symmetry axis (Fig. 4; Movies S7, S8). The cuboid data revealed dynamic regions of VP2 and more stable density for VP1/3 for the inactive DLPs. The core region was similarly disordered as seen in the 5-fold axis analysis and lacking distinguishable features. As the VP1/3 region, now visible (Fig. 4A, B), was not defined in the 5-fold axis study the recovered information provides a nice complement to the otherwise single mode visualization method.

Density that defined the transcriptionally-active DLP structure was similar in signal within the VP6 region to the inactive particle but varied in the VP2 and VP1/3 localities. VP2 was disordered in the transcriptionally-active DLP structure while VP1/3 adopted a star-shaped configuration that flanks the well-defined center density (Fig. 4C, D). The significance of this structural rearrangement among the active particles suggests that allosteric effects during transcription affect protein structures along the 5-fold axis differently than the interfaces that are defined along the 2-fold symmetry axis.

3. Conclusions

3.1. DLPs – Active to the Core

Cryo-EM structures of actively-transcribing and inactive rotavirus DLPs demonstrated broad internal structural changes that occur during biochemical activation. Specifically, we observed that upon incubation of DLPs in buffer containing NTPs and Mg^{2+} , extensive rearrangements of the protein/RNA architecture occurred. Of particular note were the changes in high density features along the 5-fold axis of symmetry and the significant increase in density at the center of the particle. The high-density structure nearest to the VP2 layer appeared as a smooth barrel shape with a radial depth of ~ 54 Å. Further toward the center of the active DLP, another high-density structure with a radial depth of ~ 64 Å was formed in the shape of a pentameric cap that extended inward to the high-density core. This structure has a similar morphology to that of the reovirus pentameric capping enzyme $\lambda 2$ [3].

The overall architecture of active DLPs also appeared distinct from inactive DLPs along the 2-fold symmetry axis. Strong density features appeared to organize into a star-like shape that is freestanding except for 2 “arms” tethered toward the DLP interior. The high density along the 2-fold axis of inactive DLPs exhibit a perpendicular interlocking “arm” and “loop” shape. Taken together, these studies demonstrate that upon activation of transcription, rearrangement of the protein/RNA architecture occurs within the rotavirus DLP. Large areas of high density along the 5-fold axis push further inward creating a dense sphere at the center of the virus, which is possibly condensed RNA.

3.2. Structural Morphogenesis and Therapeutic Potential

The changes in density arrangement within the DLP upon activation of transcription can be viewed by morphing cross-sections of inactive and active DLP reconstructions. These computational procedures

revealed a surprising spectrum of rigidity in the biological complexes. The use of *in vitro* chemically-induced activation methods may thereby be used as an essential tool to dissect the nuanced structural rearrangements that accompany biochemical processes.

In summary, we investigated the global dynamics of DLP assemblies beyond local changes in individual protein conformations. Unique perturbations occurred within dense core regions along the five-fold and two-fold axis of the DLP structure, revealing how the VP1/3 plug region influences neighboring domains during activation. These results reinforce our earlier observations that transcriptionally active DLPs exhibit disordered capsids while having ordered interiors. This inverse relationship suggests a disorder-induced activation model, which was recently confirmed by other cryo-EM studies [10,12]. As our work continues to probe this disorder-induced activation principle, we can now trace its origins to the inner depths of the particle. We are now testing this model in other viral systems. Overall, these findings underscore the importance of examining structural perturbations of viral pathogens in action, laying the groundwork for future drug targeting approaches based on internal dynamics inherent to active biological behavior.

4. Materials and Methods

4.1. DLP Preparation and *In Vitro* Chemical Activation

Rotavirus (strain SA11-4F) DLPs were prepared as described previously [21,22]. DLPs were purified by isopycnic centrifugation in cesium chloride at a density of 1.38 g/cm^3 . For transcription reactions, $1 \mu\text{g}$ DLPs, 100 mM Tris-HCl pH 7.5, 6 mM MgAc, 4 mM DTT, 2 mM each of ATP, GTP, CTP, UTP, and $1 \mu\text{L}$ RNasin (Promega) were combined and the reaction proceeded for 30 min at 37°C . Transcription reactions were then applied to Affinity grids.

4.2. Affinity Grid Capture of DLPs

Affinity capture experiments for DLPs were conducted as previously described using EM holey carbon grids (C-flat-2/1 grids; Protochips, Inc.) functionalized with Nickel-nitrilotriacetic acid (Ni-NTA) [14,21]. The Ni-NTA layers were composed of 25% Ni-NTA lipids and 75% 1,2-dilauryl-phosphatidylchlorine filler lipids (Avanti Polar Lipids). Protein adaptors were sequentially added to the Ni-NTA coated grids. His-tagged Protein A (0.01 mg/mL) (Abcam) in buffer solution containing 50 mM HEPES, pH 7.5, 150 mM NaCl, 10 mM $MgCl_2$ and 10 mM $CaCl_2$ was added in $3 \mu\text{L}$ to the Ni-NTA coated grids and incubated for 1 min and excess solution was blotted with filter paper. VP6-specific polyclonal antisera ($\#53963$) (0.01 mg/mL) in the same HEPES buffer solution was added in $3 \mu\text{L}$ aliquots and incubated for 1 min on the Protein A decorated grids. Excess solution was removed using a Hamilton syringe. Non-transcribing and transcribing DLPs ($2 \mu\text{L}$ of mg/mL) were added to the antibody-decorated grids for 2 min. Frozen-hydrated specimens were prepared by plunge-freezing the grids into liquid ethane slurry using a Cryoplunge™ 3 equipped with Gentle Blot capabilities (Gatan, Inc.) while using a one-sided blotting routine for 8 s.

4.3. Cryo-EM Data Collection

Frozen-hydrated specimens were transferred to a 626 Cryo holder (Gatan, Inc.) and maintained in liquid nitrogen until transferred to the TEM. DLPs were imaged using FEI Tecnai Spirit Biotwin TEM (FEI Co.) equipped with a LaB₆ filament and operated at acceleration voltage of 120 kV under low-dose conditions ($\sim 5 \text{ electrons}/\text{Å}^2$). Images of inactive and transcriptionally-active DLPs were recorded on a FEI Eagle 2 k HS CCD camera with a pixel size of $30\text{-}\mu\text{m}$. Defocus values of the images ranged from -1 to $-3.0 \mu\text{m}$ and images were recorded at a nominal magnification of $68,000\times$, for a final sampling of $\sim 4.4 \text{ Å/pixel}$ at the specimen level.

4.4. Image Processing and 3D Reconstructions

The RELION software package was used to calculate 3D structures of rotavirus DLPs according to standard procedures [16]. The contrast transfer function (CTF) was estimated using the program ctfind3. The auto-picking procedure in RELION was used to select particles based on references that were generated through 2D class averages of manually selected particles. A reference model for the rotavirus DLP structure was downloaded from the Grigorieff laboratory website and low-pass filtered at 30 Å. Three-dimensional classification routines identified 5 classes while enforcing icosahedral symmetry over 25 cycles of refinement. Overall parameters for global reconstruction routines included a pixel size of 4.4 Å, CTF-correction, and a regularization parameter of $T = 4$ over an angular space of 7.5 degrees. The resolution of the resulting structures was verified using the RMEASURE program [21] and assessed at the 0.5-FSC standard. Density maps were analyzed using the UCSF Chimera software package [16] and movies were generated using standard cross-section and rotational scripts in Chimera as previously noted.

Supplementary data to this article can be found online at <https://doi.org/10.1016/j.csbj.2019.07.019>.

Declaration of Competing Interest

The authors claim no conflicts of interest.

Acknowledgements

This work was supported by the National Institutes of Health, the National Cancer Institute, and the National Institute of Allergy and Infectious Disease through funding sources R01CA193578 to D.F.K and R01AI116815 to S.M.M. Cryo-EM maps have been deposited in the EMDataBank for the inactive DLP structure (EMD-20592) and the transcriptionally active DLP structure (EMD-20593).

References

- [1] Crawford SE, Ramani S, Tate JE, Parashar UD, Svensson L, Hagbom M, et al. Rotavirus infection. *Nat Rev Dis Primers* 2017;3:17083.
- [2] Trask SD, McDonald SM, Patton JT. Structural insights into the coupling of virion assembly and rotavirus replication. *Nat Rev Microbiol* 2012;10:165–77.
- [3] Reinisch KM, Nibert ML, Harrison SC. Structure of the reovirus core at 3.6 Å resolution. *Nature* 2000;404:960–7.
- [4] McClain B, Settembre E, Temple BRS, Bellamy AR, Harrison SC. X-ray crystal structure of the rotavirus inner capsid particle at 3.8 Å resolution. *J Mol Biol* 2010;397:587–99.
- [5] Lawton JA, Estes MK, Prasad BV. Mechanism of genome transcription in segmented dsRNA viruses. *Adv Virus Res* 2000;55:185–229.
- [6] Jayaram H, Estes MK, Prasad BVV. Emerging themes in rotavirus cell entry, genome organization, transcription and replication. *Virus Res* 2004;101:67–81.
- [7] Lawton JA, Estes MK, Prasad BV. Three-dimensional visualization of mRNA release from actively transcribing rotavirus particles. *Nat Struct Biol* 1997;4:118–21.
- [8] Li Z, Baker ML, Jiang W, Estes MK, Prasad BVV. Rotavirus architecture at subnanometer resolution. *J Virol* 2009;83:1754–66.
- [9] Chen JZ, Settembre EC, Aoki ST, Zhang X, Bellamy AR, Dormitzer PR, et al. Molecular interactions in rotavirus assembly and uncoating seen by high-resolution cryo-EM. *Proc Natl Acad Sci U S A* 2009;106:10644–8.
- [10] Ding K, Celma CC, Zhang X, Chang T, Shen W, Atanasov I, et al. In situ structures of rotavirus polymerase in action and mechanism of mRNA transcription and release. *Nat Commun* 2019;10:2216.
- [11] Estrozi LF, Settembre EC, Goret G, McClain B, Zhang X, Chen JZ, et al. Location of the dsRNA-dependent polymerase, VP1, in rotavirus particles. *J Mol Biol* 2013;425:124–32.
- [12] Jenni S, Salgado EN, Herrmann T, Li Z, Grant T, Grigorieff N, et al. In situ structure of rotavirus VP1 RNA-dependent RNA polymerase. *J Mol Biol* 2019;431(17):3124–38 [epub ahead of print].
- [13] McDonald SM, Patton JT. Rotavirus VP2 core shell regions critical for viral polymerase activation. *J Virol* 2011;85:3095–105.
- [14] Rahimi A, Varano AC, Demmert AC, Melanson LA, McDonald SM, Kelly DF. A non-symmetric reconstruction technique for transcriptionally-active viral assemblies. *J Anal Mol Tech* 2015;2.
- [15] Cohen J. Ribonucleic acid polymerase activity associated with purified calf rotavirus. *J Gen Virol* 1977;36:395–402.
- [16] Scheres SHW. RELION: implementation of a Bayesian approach to cryo-EM structure determination. *J Struct Biol* 2012;180:519–30.
- [17] Pettersen EF, Goddard TD, Huang CC, Couch GS, Greenblatt DM, Meng EC, et al. UCSF chimera—a visualization system for exploratory research and analysis. *J Comput Chem* 2004;25:1605–12.
- [18] Prasad BV, Rothnagel R, Zeng CQ, Jakana J, Lawton JA, Chiu W, et al. Visualization of ordered genomic RNA and localization of transcriptional complexes in rotavirus. *Nature* 1996;382:471–3.
- [19] Goddard TD, Huang CC, Ferrin TE. Visualizing density maps with UCSF chimera. *J Struct Biol* 2007;157:281–7.
- [20] Prasad BV, Wang GJ, Clerx JP, Chiu W. Three-dimensional structure of rotavirus. *J Mol Biol* 1988;199:269–75.
- [21] Kam J, Demmert AC, Tanner JR, McDonald SM, Kelly DF. Structural dynamics of viral nanomachines. *Technology*. World Scientific Publishing Co; 2014. p. 44–8.
- [22] Sousa D, Grigorieff N. Ab initio resolution measurement for single particle structures. *J Struct Biol* 2007;157:201–10.